ChemInform Abstract: Preparation and Characterization of a Stable FeSO 4 F-Based Framework for Alkali Ion Insertion Electrodes.

ARTICLE · OCTOBER 2012

DOI: 10.1021/cm302428w

9 AUTHORS, INCLUDING:

Jean-Noël Chotard
Université de Picardie Jules Verne
57 PUBLICATIONS **1,200** CITATIONS
SEE PROFILE

Christine Frayret
Université de Picardie Jules Verne
28 PUBLICATIONS **254** CITATIONS
SEE PROFILE

Sathiya Mariyappan
International Advanced Research Centre for …
27 PUBLICATIONS **824** CITATIONS
SEE PROFILE

Brent Melot
Université de Picardie Jules Verne
54 PUBLICATIONS **831** CITATIONS
SEE PROFILE

CHEMISTRY OF MATERIALS

Article

pubs.acs.org/cm

Preparation and Characterization of a Stable $FeSO_4F$-Based Framework for Alkali Ion Insertion Electrodes

Nadir Recham,[†,‡] Gwenaëlle Rousse,[§] Moulay T. Sougrati,[‡,∥] Jean-Noël Chotard,[†,‡] Christine Frayret,[†,‡] Sathiya Mariyappan,[†,‡] Brent C. Melot,[†,⊥] Jean-Claude Jumas,[‡,∥] and Jean-Marie Tarascon*[,†,‡]

[†]Laboratoire de Réactivité et Chimie des Solides (LRCS), Université de Picardie Jules Verne, CNRS UMR 7314, 33 rue Saint Leu, 80039 Amiens, France

[‡]ALISTORE-European Research Institute, 80039 Amiens, France

[§]Institut de Minéralogie et de Physique des Milieux Condensés (IMPMC), Université Pierre et Marie Curie, CNRS UMR 7590, 4 Place Jussieu, 75252 Paris Cedex 05, France

[∥]Institut Charles Gerhardt, CNRS UMR5253, Université Montpellier 2, 34095 Montpellier, France

[⊥]Department of Chemistry, University of Southern California, Los Angeles, California 90089, United States

Supporting Information

ABSTRACT: Polyanionic electrode materials offer an attractive combination of safety benefits and tunable redox potentials. Thus far, phosphate-based phases have drawn the most interest with a subsequent surge of activity focused on the newly discovered family of fluorosulfate phases. Here, we report the preparation of a new potassium-based fluorosulfate, $KFeSO_4F$, which, with removal of K, leads to a new polymorph of $FeSO_4F$ crystallizing in the high-temperature structure of $KTiOPO_4$. This new phase which contains large, empty channels, is capable of reversibly inserting 0.9 Li^+ per unit formula and can accommodate a wide variety of alkali ions including Li^+, Na^+, or K^+. This finding not only expands the rich crystal chemistry of the fluorosulfate family but further suggests that a similar strategy can apply to other K-based polyanionic compounds in view of stabilizing new attractive host structures for insertion reactions.

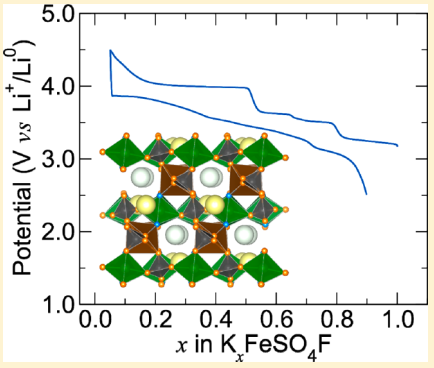

KEYWORDS: *fluorosulfates, batteries, cathode, crystal structure*

INTRODUCTION

Lithium-ion batteries power a wide spectrum of devices ranging from portable electronic devices to electric automobiles and are now essential to society. Unfortunately, they currently face significant limitations in their specific energy density which must be overcome if they are to be used in larger scale applications. To help meet this demand, there has been intense research activity in the development of high-voltage electrode materials in recent years. Starting in 2003, Barker et al. began to explore phases which contained the phosphate group (PO_4^{3-}) and fluorine (F^-) anions, out of which the *tavorite* phase of $LiVPO_4F$ was the most attractive, demonstrating a redox potential around 4.2V vs Li^+/Li.[1,2] This work also led to the discovery of $LiFePO_4F$, which presented advantages in terms of sustainability, but its open circuit voltage of 2.8 V vs Li^+/Li was too low to be useful in commercial applications.[3,4]

By simply exploiting the inductive effect associated with the increased electronegativity of different polyanionic groups,[5] we recently synthesized a new family of fluorosulfates with general formula A_xMSO_4F (A = Li, Na, M = 3d metals). Among these, the *tavorite* phase of $LiFeSO_4F$ presents an attractive redox potential at 3.6 V vs Li^+/Li.[6] Practically unknown two years ago, this family has now grown to contain more than 15 distinct compounds. Depending on the nature of the alkali metal (Li or Na), the 3d transition metal, and the synthesis conditions, the individual compositions can be crystallized in the *tavorite-*, *maxwellite-*, *triplite-*, or *sillimanite*-type structures each with different redox potentials when assembled in Li-ion batteries.[7−10] For instance, when $LiFeSO_4F$ crystallizes in the *triplite* form, it shows reversible insertion of Li^+ at 3.9 V vs Li^+/Li, the highest potential ever reported for the Fe^{3+}/Fe^{2+} redox couple in any Fe-based inorganic compounds.

Pursuing this type of investigation we decided to explore the K-based fluorosulphate members with the hope to stabilize new structures with attractive electrochemical performances when used as positive electrode materials. Here we report the successful synthesis of three new $KMSO_4F$ (M = Fe, Co, Ni) phases with special attention paid to the Fe-based phase which presents interesting chemistry toward the removal and reinsertion of K and can even accommodate the uptake of Li or Na ions as well.

Received: July 31, 2012
Revised: October 15, 2012

   dx.doi.org/10.1021/cm302428w | *Chem. Mater.* XXXX, XXX, XXX−XXX

Table 1. Crystallographic Data and Atomic Positions of $KFeSO_4F$[a]

$KFeSO_4F$						
space group $Pna2_1$		χ^2 = 2.87			R_{Bragg} = 2.66%	
a = 13.1512(1) Å		b = 6.5393(1) Å	c = 10.8689(1) Å		V = 934.716(4) Å^3	
atom	Wyckoff site	x	y	z	Biso Å^2	BVS
Fe1	4a	0.37422(8)	0.4975(3)	0	0.45(2)	2.07(2)
Fe2	4a	0.24860(18)	0.2554(3)	0.2533(4)	0.45(2)	2.03(2)
F1	4a	0.2501(5)	0.5358(12)	0.8822(5)	0.01(8)	1.01(1)
F2	4a	0.2714(4)	0.4942(14)	0.1339(6)	0.01(8)	0.98(1)
S1	4a	0.5000(4)	0.3409(3)	0.2502(6)	0.71(3)	6.04(7)
O1	4a	0.4822(8)	0.4799(13)	0.1520(7)	0.46(4)	2.30(5)
O2	4a	0.5165(9)	0.4723(14)	0.3654(7)	0.46(4)	1.90(4)
O3	4a	0.4134(5)	0.2083(11)	0.2839(7)	0.46(4)	2.00(3)
O4	4a	0.5895(5)	0.2092(10)	0.2415(7)	0.46(4)	1.91(3)
S2	4a	0.1805(2)	0.5039(7)	0.4999(6)	0.71(3)	5.82(7)
O5	4a	0.1054(5)	0.3247(10)	0.5185(8)	0.46(4)	1.80(3)
O6	4a	0.1170(6)	0.6780(11)	0.4634(7)	0.46(4)	1.87(4)
O7	4a	0.2400(6)	0.5133(17)	0.6312(7)	0.46(4)	1.65(3)
O8	4a	0.2505(6)	0.4699(14)	0.4107(8)	0.46(4)	2.58(6)
K1	4a	0.3720(2)	0.7732(4)	0.2949(3)	2.00(4)	1.14(1)
K2	4a	0.1058(2)	0.6981(3)	0.0530(3)	2.00(4)	0.90(1)

[a]Results from the Rietveld refinement against synchrotron diffraction (λ = 0.41311 Å). Bond Valence Sums (BVS) are also given.

Table 2. Crystallographic Data and Atomic Positions of $KCoSO_4F$ and $KNiSO_4F$[a]

		$KCoSO_4F$				$KNiSO_4F$			
		space group	$Pna2_1$			space group	$Pna2_1$		
		a = 13.0514(1) Å	χ^2 = 10.3			a = 12.8863(1) Å	χ^2 = 1.72		
		b = 6.4969(1) Å	R_{Bragg} = 2.23%			b = 6.4208(1) Å	R_{Bragg} = 5.97%		
		c = 10.7180(1) Å				c = 10.6284(1) Å			
		V = 908.808(4) Å^3				V = 879.397(5) Å^3			
atom	Wyckoff site	x	y	z	BVS	x	y	z	BVS
M1	4a	0.3751(2)	0.4978(5)	0	2.01(3)	0.3757(2)	0.4965(5)	0	2.0(2)
M2	4a	0.2513(3)	0.2531(6)	0.2521(6)	2.12(3)	0.2519(2)	0.2553(5)	0.2516(6)	2.0(3)
F1	4a	0.2584(10)	0.5268(17)	0.8866(11)	1.03(2)	0.2536(10)	0.529(2)	0.8793(10)	1.02(2)
F2	4a	0.2679(9)	0.5032(18)	0.1414(12)	0.99(2)	0.2731(8)	0.497(2)	0.1329(10)	1.02(2)
S1	4a	0.5065(6)	0.3360(6)	0.2563(9)	6.20(12)	0.5036(5)	0.3361(5)	0.2486(9)	5.82(10)
O1	4a	0.4897(12)	0.4641(18)	0.1526(11)	2.28(7)	0.4977(8)	0.4584(16)	0.1349(10)	2.13(6)
O2	4a	0.5195(11)	0.487(2)	0.3610(9)	1.99(5)	0.5224(9)	0.5074(19)	0.3538(10)	1.71(4)
O3	4a	0.4095(9)	0.2117(17)	0.2687(11)	1.91(5)	0.4046(9)	0.2088(18)	0.2834(11)	1.85(4)
O4	4a	0.5903(9)	0.202(2)	0.2227(14)	1.99(6)	0.5845(8)	0.1936(17)	0.2412(13)	2.19(6)
S2	4a	0.1788(3)	0.4952(14)	0.5025(9)	5.89(12)	0.1796(3)	0.4962(10)	0.5012(8)	5.64(10)
O5	4a	0.1032(9)	0.3281(16)	0.5265(12)	2.00(5)	0.1037(9)	0.3357(16)	0.5124(13)	2.20(6)
O6	4a	0.1200(9)	0.6821(18)	0.4834(13)	1.96(6)	0.1168(10)	0.6925(17)	0.4668(11)	1.66(5)
O7	4a	0.2398(10)	0.543(2)	0.6112(15)	2.18(8)	0.2442(10)	0.513(2)	0.6208(12)	1.89(5)
O8	4a	0.2538(11)	0.457(2)	0.3932(15)	1.93(6)	0.2560(9)	0.4464(18)	0.3981(13)	2.07(6)
K1	4a	0.3720(3)	0.7686(6)	0.2971(5)	1.14(15)	0.3726(3)	0.7746(7)	0.2963(5)	1.25(2)
K2	4a	0.1064(3)	0.6955(5)	0.0562(5)	0.89(12)	0.1075(3)	0.6918(6)	0.0537(5)	1.07(13)

[a]Results from the Rietveld refinement against synchrotron diffraction (λ = 0.41311 Å). Bond Valence Sum analysis (BVS) is also indicated.

EXPERIMENTAL SECTION

Synthesis. $KMSO_4F$ was prepared by ball-milling equimolar ratios of KF and $MSO_4{\cdot}H_2O$ for one hour in a SPEX 8000 M and subsequently pressing at 10 tons of pressure to form a pellet. These pellets were placed inside Teflon-lined Parr reactors that were sealed inside an Ar-filled glovebox and slowly heated at a rate of 2°C·min^{-1} to a temperature between 270 and 290 °C depending on the transition metal and annealed for 40 to 45h. A reaction temperature of 290 °C was sufficient to produce single-phased $KCoSO_4F$ and $KNiSO_4F$ powders; yet, in contrast, attempts to prepare $KFeSO_4F$ at the same temperature always produced pellets with a red coloration indicative of oxidation with no signs of the target phase. To prevent oxidation, anhydrous $FeSO_4$ was prepared by dehydrating $FeSO_4{\cdot}H_2O$ at 280 °C under vacuum for three hours. The resulting powder was ball-milled with KF for one hour, pressed into a pellet, sealed inside a quartz tube, and annealed at temperatures ranging from 300 to 400 °C in steps of 10 °C. It was found that single-phased $KFeSO_4F$ could only be obtained for temperatures near 380 °C for heating times greater than 4 days (SI Figure 1). In the process, it was found that the Co and Ni phases could also be made *via* the same process with the anhydrous precursor, suggesting that, unlike the *tavorite* phase,[6] the reaction is

dx.doi.org/10.1021/cm302428w | *Chem. Mater.* XXXX, XXX, XXX–XXX

principally governed by solid-state diffusion rather than through a topotactic substitution. The thermal stability of these $KMSO_4F$ phases was checked by thermogravimetric analysis. We found (SI Figure 2) that the Co and Ni phases decompose at lower temperatures, 300 and 350 °C, respectively, than the Fe-phase which remained stable up to 450 °C. This could explain the problems encountered in making the $KFeSO_4F$ phase as the range of temperature over which it could be formed is limited since it decomposes over 450 °C but does not start to form until 370 °C.

Characterization. *X-ray Diffraction.* X-ray diffraction (XRD) patterns were recorded using two separate Bruker D8 diffractometers. The first one was equipped with a Co−Kα radiation source (λ_1 = 1.78897 Å, λ_2 = 1.79285 Å) with a Vantec detector, while the other used a Cu−Kα radiation source (λ_1 = 1.54056 Å, λ_2 = 1.54439 Å) with a Lynxeye detector. Both were operated at 40 kV and 40 mA. High-resolution synchrotron powder diffraction patterns were collected through the mail-in program at the 11-BM beamline at the Advanced Photon Source (Argonne National Lab) using a wavelength of 0.41311 Å. The powders sent to 11-BM were sealed under Ar in glass capillaries with a 0.5 mm diameter. The powder patterns were refined using the Rietveld method[11] as implemented in the FullProf program.[12]

Structure Determination. The Bragg positions and observed extinctions for the as-prepared phases were recognized to be consistent with the orthorhombic $Pna2_1$ space group with lattice parameters similar to those reported for $KTiOPO_4$ (KTP). The structure was therefore refined by starting from the structural model of KTP[13] but replacing the unit-cell parameters with those obtained by indexing the observed reflections in the synchrotron data set. The results of this refinement are presented in Table 1 for the Fe-based compound and Table 2 for the Co and Ni counterparts. After receiving the 11-BM data, samples of $KCoSO_4F$ were obtained with higher purity so the results of this refinement against laboratory XRD are shown in Figure 1 (a). A bond valence sum (BVS) analysis employing the Zachariasen formula $V_i = \Sigma_j s_{ij} = \Sigma_j \exp((d_0-d_{ij})/0.37)$ using the d_0 parameter taken from ref 14 was conducted. Note the good agreement between the BVS and the expected charge on the atoms in Table 1. Given that the KTP structure crystallizes in the $Pna2_1$ space group, it does not contain a center of inversion symmetry and therefore possesses a floating origin along the *c*-axis. We have, therefore, fixed the origin of the cell on one of the two independent transition metal sites in the structure by fixing the z-coordinate to zero.

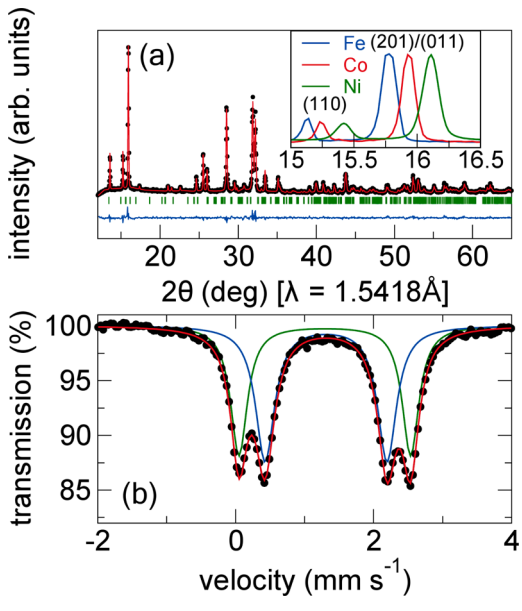

Figure 1. (a) Results of the Rietveld refinement of the X-ray diffraction pattern of $KCoSO_4F$ black circles, red lines, and blue lines represent the observed, calculated, and difference patterns, respectively (λ_{Cu}). The expected positions of the Bragg reflections are shown as vertical green bars. The inset shows the shift of the (110), (201), and (011) reflections for the different analogues as expected for the different ionic radii of Fe^{2+}, Co^{2+}, and Ni^{2+}. (b) Room temperature Mössbauer spectrum of $KFeSO_4F$. The green and blue doublets are assigned to Fe1 and Fe2, respectively, which are divalent cations.

Electrochemical Tests. Electrochemical cells were assembled using positive electrodes which consisted of a hand-mixed composite of 80:20 weight ratio of $KFeSO_4F$ and carbon SP. Metallic Li foil was used as the negative electrode and a Whatman GF/D borosilicate glass fiber sheet saturated with 1 M $LiPF_6$ in ethylene carbonate (EC), propylene carbonate (PC), and dimethyl carbonate (DMC) (1:1:3 w/w) as the electrolyte. The coverage of the current collector was typically around 6 mg·cm^{-2}, and all cells were started on oxidation unless otherwise stated.

Mössbauer Spectroscopy. Room temperature Mössbauer measurements were carried out using a standard constant acceleration geometry with a 0.5 Gbq source of ^{57}CoRh. Absorbers were made by mixing 20 mg of the compounds with 60 mg of boron nitride. *In situ* and *in operando* Mössbauer measurements were collected using the same stainless steel Swagelok-type cell as for XRD with a special plunger which enabled the γ rays to be passed through the powder. All isomer shifts are quoted with respect to an α-Fe reference at room temperature.

RESULTS

The XRD patterns for the Fe, Co, and Ni analogues are very similar and reflect the fact that all the compositions adopt the same structure. The most significant difference can be seen in the inset of Figure 1 (a) which shows the shift of some Bragg peaks toward lower angles in 2θ reflecting the increased lattice parameters that result from the increasing ionic radius of Ni (r = 0.69 Å), Co (r = 0.745 Å), and Fe (r = 0.78 Å).[15]

The structure of the as-prepared compounds, illustrated in Figure 2(a), (b), and (c), consists of chains of MO_4F_2 octahedra which are linked through their vertices *via* F atoms. The fluorine atoms in the MO_4F_2 octahedra alternate their orientation between a *cis* and *trans* position along the length of the chains corresponding to the green and brown octahedra, respectively, in Figure 2(c). Moreover, two SO_4 groups bridge adjacent octahedra along the length of the chains which forces the chains, which run along the [011] and [0−11] directions of the unit cell, to be much more buckled in $KMSO_4F$ than in the Li- or Na-based polymorphs. As seen in Figure 2(a) and 2(b), the packing of these chains creates two large cavities along the [100] and [010] directions filled by either K1 or K2, respectively. Compared to those found in the *tavorite*, which are approximately 4 Å × 2.6 Å, the cavities depicted here are significantly larger (about 4.3 Å × 4.8 Å), thus offering much more space to accommodate the K ions. Clearly, the large ionic radius of K plays a key role in forcing $KMSO_4F$ to adopt a structure so distinct from the other fluorosulfate phases. Overall, from a structural point of view, $KFeSO_4F$ does not appear to be topologically related to *tavorite*-$LiFeSO_4F$ or $FeSO_4{\cdot}H_2O$, which explains why its formation can be achieved using anhydrous precursors.

Mössbauer spectroscopy was employed in an attempt to discern the difference between the Fe environments where F ions are oriented in the *cis versus trans* positions. Indeed, the spectrum shown in Figure 1(b) contains a set of two doublets indicating two inequivalent environments in agreement with the structure determined using diffraction. The two doublets exhibit comparable isomer shifts around 1.29 and 1.31 mm·s^{-1} for the outer and inner doublets, respectively; this indicates that

dx.doi.org/10.1021/cm302428w | Chem. Mater. XXXX, XXX, XXX−XXX

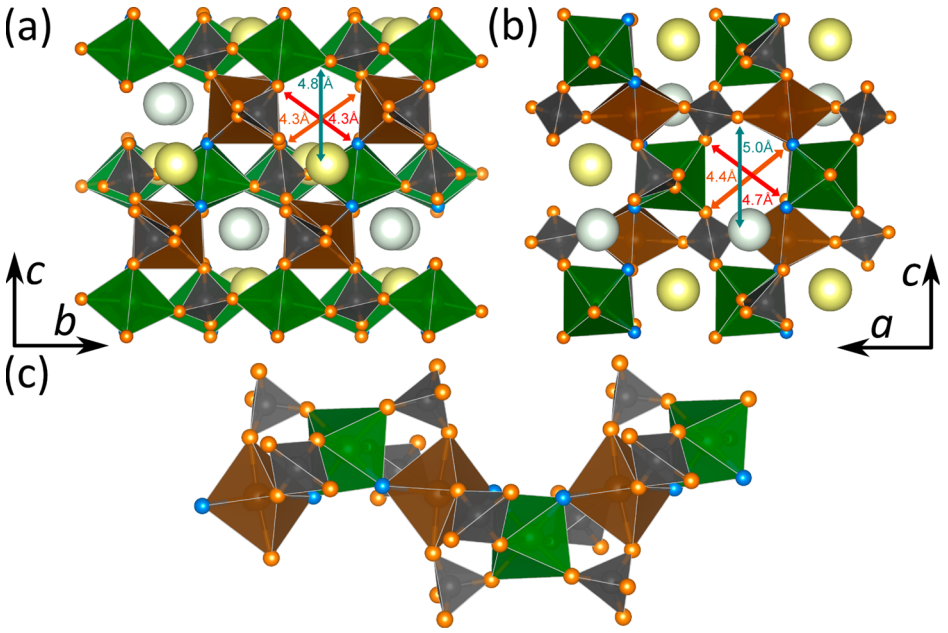

Figure 2. Illustration of the crystal structure of $KMSO_4F$: (a) view down the *a*-axis of the unit cell and (b) view down the *b*-axis of the unit-cell. *M* atoms are at the center of the green (*M*1) and brown (*M*2) octahedra, oxygen is in orange, sulfate groups are in gray, K are displayed as yellow (K1) and gray (K2) spheres, and fluorine atoms are blue. The size of the tunnels where K sits is also indicated. (c) Chains of corner-sharing MO_4F_2 octahedra in $KMSO_4F$. Note that F atoms are successively in *cis* (green octahedra) and *trans* (brown octahedra) positions along the chains.

the Fe^{2+} ions adopt a high spin configuration.[16] In contrast, the two doublets show different quadrupole splittings of 2.49 and 1.78 mm s^{-1}. When the distortion of each site is taken into account, the outer and inner doublets are believed to correspond to the Fe1 and Fe2 sites respectively. It should also be noted that there was no evidence of any contribution from Fe^{3+}, confirming the purity of the prepared materials.

The presence of such large channels in the structure motivated an investigation of the electrochemical properties which focused primarily on the Fe-based fluorosulfate. The voltage-composition profile, shown in Figure 3, indicates that it is possible to completely remove all of the K ions from $KFeSO_4F$ as the cell is charged to 4.5 V with a Li-foil as the negative electrode. This change in voltage as K is removed; however, does not increase smoothly but rather shows a staircase-like behavior with each step likely to reflect a change in the structure. To gain further insight into the evolution of the structure, *in situ* XRD and Mössbauer data were collected, the results of which are illustrated in Figure 3. The XRD patterns confirm the presence of single phase regions for values of $x = 1$, 0.80, 0.55, and 0.10 in K_xFeSO_4F. These points correlate well with the sharp increases observed in the potential with the exception of $x = 0.65$ where a prominent change can be seen in the voltage but not in the XRD pattern. During the first stage of oxidation ($0.55 \leq x \leq 1$), successive biphasic domains and solid solutions can be seen with peaks shifting and significant changes in intensity, in agreement with the three plateaus separated by sloped curves in the voltage profile. The full XRD powder patterns (which can be found in SI Figure 3) clearly indicate the existence of a biphasic domain during the second part of oxidation where peaks associated with the $x = 0.10$ phase grow at the expense of the peaks associated with the $x = 0.55$ phase. The process for the deintercalation of K is summarized in Figure 4(a) by plotting the volume of the unit cell during the oxidation.

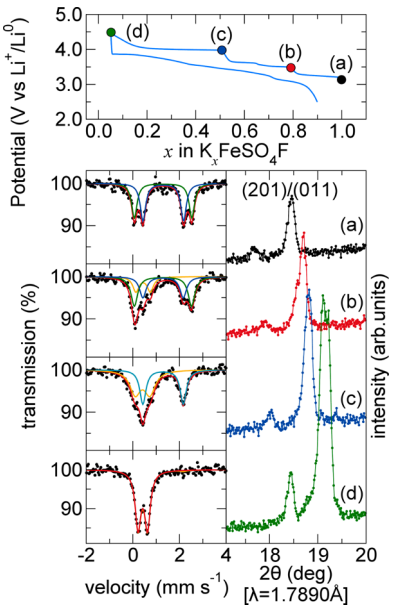

Figure 3. Top panel: Electrochemical curve of a Li/$KFeSO_4F$ cell started on charge. Bottom panel: typical *in situ* Mössbauer spectra (left) and XRD patterns (right) recorded during the first oxidation at positions (a) to (d) as indicated on the voltage profile.

Curiously, the intensities of the (011)/(201) doublet at $d \approx 5.6$ Å (corresponding to $2\theta \approx 18°$, see Figure 3, right) were found to significantly increase with removal of K ions, whereas the intensity of the (212) peak rapidly decreases to zero. However, a closer inspection of the structure factor for these reflections confirms that the large atomic scattering factor of K should indeed be expected to cause this kind of change in intensities. These three peaks can therefore be used as a means to monitor the K content during oxidation. It should also be noted that the existence of two crystallographic sites for K in

dx.doi.org/10.1021/cm302428w | *Chem. Mater.* XXXX, XXX, XXX–XXX

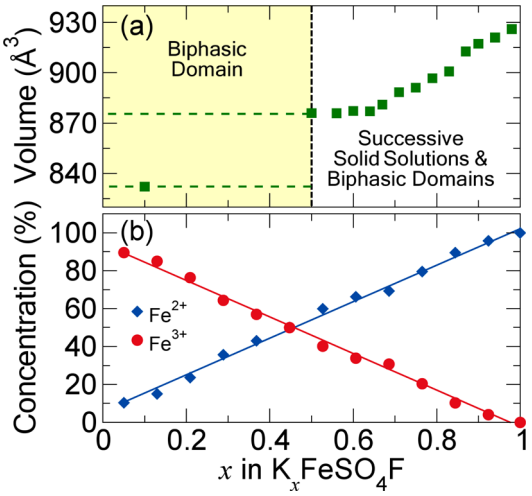

Figure 4. (a) Evolution of the unit cell volume, obtained from a profile matching of each pattern during the *in situ* XRD data collection (b) Fe^{2+} and Fe^{3+} concentrations obtained from *in situ* Mössbauer during the first oxidation of a Li/$KFeSO_4F$ cell.

the structure implies a possibly preferential removal from one site or the other. Indeed, this could also explain the existence of so many intermediate phases, corresponding to the different voltage steps, as the K1 and K2 sites depopulate and stabilize new symmetries and phases. Unfortunately, the quality of the *in situ* XRD was insufficient to accurately determine the K occupancies for each of the two sites and the exact potassium positions for these intermediate phases. Experiments with synchrotron radiation are currently planned to clarify the process of depopulating the two K sites on charging.

Having previously found it possible to differentiate between the two different Fe sites in the structure, Mössbauer was employed to monitor the oxidation state of Fe as K was removed. Spectra were collected during the deinsertion of K for compositions with $\Delta x = 0.077$, but only the most relevant are shown on the lower left side of Figure 3. As mentioned earlier, the spectrum for the as-prepared sample [see the Figure 1(b)] shows two different doublets corresponding to two different Fe^{2+} sites. With initial removal of potassium, the variations in the shape of the spectra indicate the two Fe sites do not oxidize equally (see SI Figure 4). The Fe2 sites were found to initially oxidize faster than the Fe1 sites, and this effect appeared to continue until $x = 0.55$, at which point the onset of a drastic structural change leads to the evolution of a new type of Fe^{2+} site at the expense of both starting Fe^{2+} sites, which fully disappear.

Further removal of K ($x < 0.5$) leads to increasing complexity in the Mössbauer spectra until the sample is fully charged (e.g., all of the K is removed) and the spectra begin to contain a single well-defined Fe^{3+} signal with IS, QS, and LW of 0.45, 0.40, and 0.29 mm s^{-1}, respectively (see Figure 3 left). Moreover, the Mössbauer spectra for K_0FeSO_4F appear very similar to the one previously collected for the delithiated *tavorite* Li_0FeSO_4F phase (IS, QS, and LW of 0.47, 0.41, and 0.28 mm s^{-1}, respectively)[17] whose structure was shown, by both neutron and synchrotron diffraction experiments,[6,18] to possess a single Fe^{3+} site. This may imply the removal of K from $KFeSO_4F$ triggers the transition from two sites to one site structure. However, no definitive conclusions can be drawn as the Mössbauer signal, while quite narrow, can be fit equally well with two Fe^{3+} sites with tiny differences in quadrupole splitting (~0.05 mm·s^{-1}).

Lastly, Mössbauer spectra were also collected on discharge (see SI Figure 5) and the concentrations of Fe^{2+} and Fe^{3+}, shown in Figure 4(b), indicate a nearly complete reduction of Fe^{3+} to Fe^{2+} indicating a fully reversible process. Nevertheless, the Mössbauer spectrum recorded at the end of the discharge is different from the as-prepared material implying the formation of a new phase. This comes as no surprise considering that the discharge voltage profile significantly differs from the one on charge (Figure 3 top).

To obtain further structural information about the oxidized phase of formula "$FeSO_4F$", $KFeSO_4F$ was chemically oxidized using NO_2BF_4 dissolved in acetonitrile. The resulting XRD pattern differs significantly from the pristine phase and is in agreement with what was observed during the *in situ* XRD experiment. A large shift in the position of the Bragg peaks toward higher angles is indicative of a decrease in the volume as expected for K departure (see inset of Figure 5). We also note

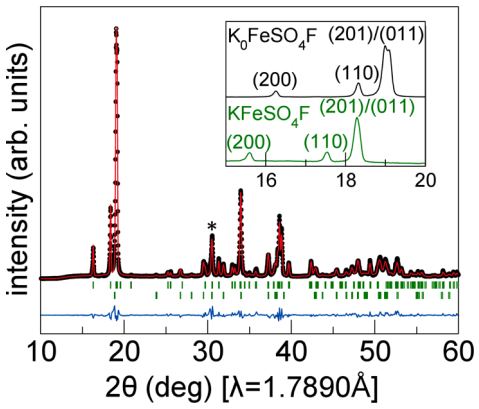

Figure 5. Rietveld refinement of the X-ray diffraction pattern of $FeSO_4F$ obtained by chemical oxidation from $KFeSO_4F$. Black circles, red lines, and blue lines represent the observed, calculated, and difference patterns, respectively (λ_{Co}). The positions of the Bragg reflections are shown as vertical green bars. 1st line: $FeSO_4F$, 2nd line: KBF_4 compound coming from the use of NO_2BF_4 as oxidant. The (*) indicates the position of the (212) peak of $KFeSO_4F$ which vanishes as K is removed. This peak is at the same position as the main peak of KBF_4. The peak shift between the pristine material (green) and the oxidized sample (black) is illustrated in the inset.

the appearance of additional peaks which could be attributed to KBF_4. Unfortunately, removal of KBF_4 is effectively impossible as it is not soluble in any solvents which would not also dissolve the oxidized phase. Despite the presence of KBF_4, the main peaks in the powder pattern are maintained which implies the framework of the new structure is topologically similar to that of the title phase with slightly smaller lattice parameters. Further, it was found that the absence of K allowed the structure to be refined in the centrosymetric *Pnna* space group, which is the space group adopted by KTP in the high temperature paraelectric phase.[19,20] The resulting structural parameters are reported in Table 3 and the Rietveld refinement is shown in Figure 5. The unit cell volume is decreased by 10.8% ($V = 834.13(2)$ Å^3) as compared to the pristine $KFeSO_4F$ phase. This new polymorph of "$FeSO_4F$" was found to be stable up to 300 °C.

Since the process of chemically oxidizing these phases leads to a mixture of $FeSO_4F$ and KBF_4, it was necessary to charge a

dx.doi.org/10.1021/cm302428w | *Chem. Mater.* XXXX, XXX, XXX–XXX

Table 3. Crystallographic Data and Atomic Positions of Chemically Oxidized $FeSO_4F$[a]

$FeSO_4F$					
space group *Pnna*		χ^2 = 9.34	R_{Bragg} = 3.87%		
a = 12.6321(2) Å		*b* = 10.5469(2) Å	*c* = 6.2609(1) Å	*V* = 834.13(2) Å^3	
atom	Wyckoff site	*x*	*y*	*z*	BVS
Fe1	4*d*	0.1335(3)	0.25	0.25	3.00(3)
Fe2	4*b*	0	0	0.5	2.83(3)
F	8*e*	0.5199(6)	0.1274(8)	0.720(2)	0.99(2)
S1	4*c*	0.25	0	0.4036(9)	6.9(9)
O1	8*e*	0.7402(8)	0.393(1)	0.772(1)	2.32(5)
O2	8*e*	0.6602(6)	0.517(1)	0.044(1)	2.07(4)
S2	4*d*	0.5554(5)	0.25	0.25	5.94(8)
O3	8*e*	0.3622(7)	0.771(1)	0.933(1)	1.98(4)
O4	8*e*	0.5058(7)	0.6410(9)	0.777(2)	1.98(5)

[a]Results from the Rietveld refinement against X-ray diffraction (λ_{Co1} = 1.78897 Å and λ_{Co2} = 1.79285 Å). Bond Valence Sum analysis (BVS) is also indicated.

cell, which was loaded with $KFeSO_4F$ as the positive electrode, up to 4.8 V to remove K and accurately assess the electrochemical performance of this new "$FeSO_4F$" polymorph. After the positive electrode was subsequently recovered, the phase was washed twice with DMC and dried prior to confirming the absence of K by EDX measurements. This material was then used as the new positive electrode of a fresh cell with a new negative electrode of Li foil. This cell, which was cycled at a rate of C/20 between 2 and 4.5 V, shows the reversible uptake of ~0.9 Li^+ per unit formula around an average voltage of ~3.7 V (Figure 6a) for at least 10 cycles. To check the practical feasibility for implementing this material in Li batteries, extended cycling has been done and we have so far achieved 70 cycles (see SI Figure 6) with limited capacity fading. Similarly $Na/FeSO_4F$ and $K/FeSO_4F$ cells were built using 1 M $NaClO_4$ and 1 M $KClO_4$ respectively in propylene carbonate as electrolyte. The voltage-composition profile for the $Na/FeSO_4F$ (Figure 6b) shows the reversible uptake of 0.85 Na^+ ion per unit formula *via* a two-step process which is more pronounced on discharge than on charge. For the cell containing a K anode, we found that $FeSO_4F$ can electrochemically uptake 0.8 K^+ ions per unit formula (Figure 6c) at a relatively high voltage and via a complex process as indicated by the numerous accidents in the discharge/charge voltage profile.

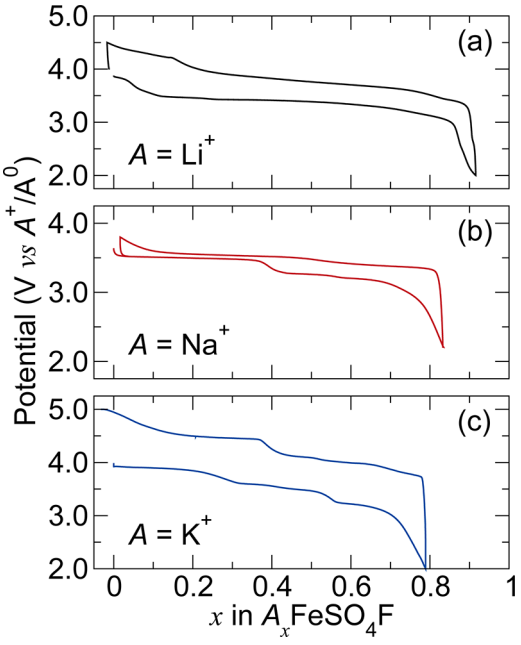

Figure 6. Electrochemical behavior of "K_0FeSO_4F", which was obtained *via* the electrochemical oxidation of $KFeSO_4F$ by assembling a $Li/KFeSO_4F$ cell (see the text for details). The recovered $FeSO_4F$ powder already containing 20% carbon additive was cycled vs Li (a), Na (b), and K (c) anodes using 1 M $AClO_4$ (*A*= Li, Na, K) in propylene carbonate electrolytes. The three cells were discharged at a current rate of C/20.

Comparing the three alkali/$FeSO_4F$ cells, we note that the polarization is the smallest for the Na-based curve, indicative of a faster insertion-deinsertion process (e.g, better electrode kinetics) which likely results from a better diffusion of the Na^+ ion atoms within the channels of the host structure. The limited rate capability in the presence of Li was confirmed by the shape of the charge-discharge curves (see SI Figure 6). This comes as no surprise as the diffusion of larger ions like K^+ could suffer from kinetic hindrances, while the diffusion of smaller ones like Li^+ are typically slowed-down by pinning interactions with the lattice. Although detailed structural and diffusion studies of the insertion-deinsertion mechanisms of Li^+, Na^+, and K^+ into $FeSO_4F$ remain to be done, the present results indicate the versatility of the new "$FeSO_4F$" polymorph as a host toward the reversible uptake of various alkali guests. This is a property shared by very few materials; among them the Chevrel phases[21,22] that, in addition to alkali (Li^+, Na^+), can accept divalent cations such as Mg^{2+}, for instance.[23]

Regarding the Ni and Co-based $KMSO_4F$ phases, their electrochemical performances were also investigated. $Li/KCoSO_4F$ and $Li/KNiSO_4F$ cells were assembled and charged to voltages of 5.2 V using 1 M $LiPF_6$ in EC-DMC electrolyte. We found (see SI Figure 6) that some K could be reversibly removed from the Co phase for voltages greater than 4.9 V and re-inserted Li^+ at a potential of ~4.6 V with a large irreversibility between the first charge and discharge due to a significant degree of electrolyte decomposition. In contrast, no sign of electrochemical capacity was obtained for the Ni-based phases. Maintaining the voltage of a $Li/KNiSO_4F$ to 5.2 V was found to lead to continuous electrolyte degradation without any residual capacity on the following discharge. This high Co^{3+}/Co^{2+} redox voltage is also in line with what should be expected since the 3*d* transition metal redox voltages are well-known and have even been predicted from DFT calculations,[24−26] to

dx.doi.org/10.1021/cm302428w | Chem. Mater. XXXX, XXX, XXX−XXX

increase with the following sequence $Fe^{3+}/Fe^{2+} < Mn^{3+}/Mn^{2+} < Co^{3+}/Co^{2+}$ and Ni^{3+}/Ni^{2+} with values usually approaching 5 V for the Co and Ni phases. Thus, electrolytes which are stable at higher potentials are needed to further exploit the higher potential of these Co- and Ni-based phases or any other high voltage polyanionic compounds.

Lastly, looking further into the structural aspects of these new $KMSO_4F$ compounds, although their KTP structure appears different from that of the Na and Li counterparts, the underlying polyanionic framework of the structures are both composed of tetrahedral SO_4 groups and isolated F ions. Figure 7 compares the different structures adopted by the

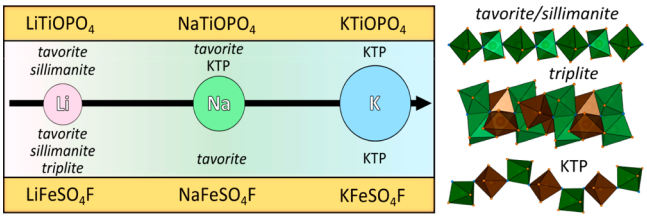

Figure 7. Left: Structural similarities between titanyl phophates and iron fluorosulfates when the alkaline cation is changed from Li to Na, and further to K. Right: topology of the transition metal chains in the different polymorphs. Fe atoms are at the center of the green or brown octahedra, oxygen is in orange, and fluorine atoms are blue. Note that for *triplite*, there is site mixing with Li on the Fe sites such that they are indistinguishable. The details of the structure for $LiTiOPO_4$,[31−33] $NaTiOPO_4$[34,35] and $KTiOPO_4$[13] were taken from the respective references.

titanyl phosphates $ATiOPO_4$ and transition metal fluorosulfates $AMSO_4F$ when the alkali metal A is changed from Li, Na, and K. It is informative to recognize that as the size of the alkali ion is increased the packing of the SO_4 groups is necessarily disrupted. Therefore, unlike *tavorite*, *sillimanite*, or *triplite* the SO_4 groups in the KTP structure are no longer capable of forming such a tightly packed network. As a result, the framework in the K-based phase appears to have significantly more void space than that of the Li- or Na-based materials. This is confirmed by the much lower calculated density (obtained from structural determination) of the KTP-like $FeSO_4F$ framework (2.72 $g{\cdot}cm^{-3}$) as compared to the *triplite* and *tavorite*-like $FeSO_4F$ frameworks (3.21 and 3.40 $g{\cdot}cm^{-3}$, respectively[18,27]). Several fluorophosphates of general formulas $KMPO_4F$ (M = Cr,[28] Fe,[29] Al[30]) have also been reported, all of which crystallize in the ferroelectric or paraelectric phases of KTP. More importantly, the results we present here suggest that searching for K-based polyanionic compounds, which can undergo an ion exchange reaction, could be a new strategy for stabilizing new alkali-free polymorphs related to KTP.

In summary, new K-based member of the fluorosulfate family, which can be synthesized at temperatures below 400 °C via solid state reactions, have been found to adopt a KTP-based structure. Of particular interest is the structural similarity between the alkali-based phosphates and fluorosulfates as they display a similar structural relationship with increasing size of the alkali ion. Additionally, the redox chemistry reveals interesting possibilities to electrochemically replace K by Li as a route to prepare new polymorphs with comparable redox activity to that of the *tavorite* polymorph. Moreover, the open $FeSO_4$-based framework pertaining to the KTP-type structure offers this phase the feasibility of reversibly uptake other alkali ions thus its possible application as a positive electrode in Na or K-based batteries. Several improvements to the present work are immediately apparent and range from electrode optimization to an alternative low temperature chemical oxidation route to prepare $FeSO_4F$ free of KBF_4. Additionally, they could enlist the insertion of divalent ions such as Mg^{2+} within the new open $FeSO_4F$ framework structure. Last, given the noncentrosymmetric space group, the potential for interesting optical/multiferroic properties of these new phases is clear and, as such, are presently under investigation.

■ ASSOCIATED CONTENT

Supporting Information

Additional details describing the results of the DFT calculations, Mossbauer spectroscopy, and TGA. CIFs (Crystallographic information files) are also available. This material is available free of charge via the Internet at http://pubs.acs.org.

■ AUTHOR INFORMATION

Corresponding Author

*E-mail: jean-marie.tarascon@sc.u-picardie.fr.

Notes

The authors declare no competing financial interest.

■ ACKNOWLEDGMENTS

We would like to thank M. Courty for conducting the TGA measurements and the French network RS2E for supporting this work.

■ REFERENCES

(1) Barker, J.; Saidi, M. Y.; Swoyer, J. L. *J. Electrochem. Soc.* **2003**, *150*, A1394−A1398.
(2) Mba, J. M. A.; Croguennec, L.; Basir, N. I.; Barker, I.; Masquelier, C. *J. Electrochem. Soc.* **2012**, *159*, A1171−A1175.
(3) Recham, N.; Chotard, J. N.; Jumas, J. C.; Laffont, L.; Armand, M.; Tarascon, J. M. *Chem. Mater.* **2010**, *22*, 1142−1148.
(4) Ramesh, T. N.; Lee, K. T.; Ellis, B. L.; Nazar, L. F. *Electrochem. Solid-State Lett.* **2010**, *13*, A43−A47.
(5) Padhi, A. K.; Nanjundaswamy, K. S.; Masquelier, C.; Goodenough, J. B. *J. Electrochem. Soc.* **1997**, *144*, 2581−2586.
(6) Recham, N.; Chotard, J. N.; Dupont, L.; Delacourt, C.; Walker, W.; Armand, M.; Tarascon, J. M. *Nat. Mater.* **2010**, *9*, 68−74.
(7) Ati, M.; Melot, B. C.; Rousse, G.; Chotard, J.-N.; Barpanda, P.; Tarascon, J.-M. *Angew. Chem., Int. Ed.* **2011**, *50*, 10574−10577.
(8) Barpanda, P.; Ati, M.; Melot, B. C.; Rousse, G.; Chotard, J. N.; Doublet, M. L.; Sougrati, M. T.; Corr, S. A.; Jumas, J. C.; Tarascon, J. M. *Nat. Mater.* **2011**, *10*, 772−779.
(9) Melot, B. C.; Chotard, J. N.; Rousse, G.; Ati, M.; Reynaud, M.; Tarascon, J. M. *Inorg. Chem.* **2011**, *50*, 7662−7668.
(10) Reynaud, M.; Barpanda, P.; Rousse, G.; Chotard, J. N.; Melot, B. C.; Recham, N.; Tarascon, J. M. *Solid State Sci.* **2012**, *14*, 15−20.
(11) Rietveld, H. M. *J. Appl. Crystallogr.* **1969**, *2*, 65−71.
(12) Rodriguez-Carvajal, J. *Physica B* **1993**, *192*, 55−69.
(13) Tordjman, I.; Masse, R.; Guitel, J. C. *Z. Kristallogr.* **1974**, *139*, 103−115.
(14) Brown, I. D.; Altermatt, D. *Acta Crystallogr., Sect. B: Struct. Sci.* **1985**, *41*, 244−247.
(15) Shannon, R. D. *Acta Crystallogr., Sect. A: Cryst. Phys., Diffr., Theor. Gen. Crystallogr.* **1976**, *32*, 751−767.
(16) Menil, F. *J. Phys. Chem. Solids* **1985**, *46*, 763−789.
(17) Ati, M.; Sougrati, M. T.; Recham, N.; Barpanda, P.; Leriche, J. B.; Courty, M.; Armand, M.; Jumas, J. C.; Tarascon, J. M. *J. Electrochem. Soc.* **2010**, *157*, A1007−A1015.

(18) Melot, B. C.; Rousse, G.; Chotard, J. N.; Ati, M.; Rodriguez-Carvajal, J.; Kemei, M. C.; Tarascon, J. M. *Chem. Mater.* **2011**, *23*, 2922−2930.
(19) Yashima, M.; Komatsu, T. *Chem. Commun.* **2009**, 1070−1072.
(20) Norberg, S. T.; Thomas, P. A.; Tucker, M. G. *J. Phys.: Condens. Matter* **2011**, *23*, 175401.
(21) Schollhorn, R. *Angew. Chem., Int. Ed. Engl.* **1980**, *19*, 983−1003.
(22) Tarascon, J. M. *J. Electrochem. Soc.* **1986**, *133*, C119−C119.
(23) Levi, E.; Gofer, Y.; Aurbach, D. *Chem. Mater.* **2010**, *22*, 860−868.
(24) Frayret, C.; Villesuzanne, A.; Spaldin, N.; Bousquet, E.; Chotard, J. N.; Recham, N.; Tarascon, J. M. *Phys. Chem. Chem. Phys.* **2010**, *12*, 15512−15522.
(25) Arroyo-de Dompablo, M. E.; Armand, M.; Tarascon, J. M.; Amador, U. *Electrochem. Commun.* **2006**, *8*, 1292−1298.
(26) Meng, Y. S.; Arroyo-de Dompablo, M. E. *Energy Environ. Sci.* **2009**, *2*, 589−609.
(27) Ati, M.; Melot, B. C.; Chotard, J. N.; Rousse, G.; Reynaud, M.; Tarascon, J. M. *Electrochem. Commun.* **2011**, *13*, 1280−1283.
(28) Slobodyanik, N. S.; Nagornyi, P. G.; Kornienko, Z. I.; Kapshuk, A. A. *Zh. Neorg. Khim.* **1991**, *36*, 1390−1392.
(29) Belokoneva, E. L.; Yakubovich, O. V.; Tsirelson, V. G.; Urusov, V. S. *Inorg. Mater.* **1990**, *26*, 505−511.
(30) Kirkby, S. J.; Lough, A. J.; Ozin, G. A. *Z. Kristallogr.* **1995**, *210*, 956−956.
(31) Geifman, I. N.; Furmanova, N. G.; Nagornyi, P. G.; Yun, L. D.; Rotenfeld, M. V. *Kristallografiya* **1993**, *38*, 88−94.
(32) Nagornyi, P. G.; Kapshuk, A. A.; Stus, N. V.; Slobodyanik, N. S.; Chernega, A. N. *Zh. Neorg. Khim.* **1991**, *36*, 2766−2768.
(33) Robertson, A.; Fletcher, J. G.; Skakle, J. M. S.; West, A. R. *J. Solid State Chem.* **1994**, *109*, 53−59.
(34) Phillips, M. L. F.; Harrison, W. T. A.; Stucky, G. D.; McCarron, E. M.; Calabrese, J. C.; Gier, T. E. *Chem. Mater.* **1992**, *4*, 222−233.
(35) Stus, N. V.; Slobodyanik, M. S.; Straitiychuk, D. A.; Lisnyak, V. V. *J. Alloys Compd.* **2005**, *393*, 66−69.